PCCP

ROYAL SOCIETY OF CHEMISTRY

PAPER

View Article Online
View Journal | View Issue

Cite this: *Phys. Chem. Chem. Phys.*, 2021, **23**, 15989

Novel copper fluoride analogs of cuprates†

Nikita Rybin, *[a] Dmitry Y. Novoselov, [abc] Dmitry M. Korotin, [ab] Vladimir I. Anisimov[abc] and Artem R. Oganov *[a]

Received 10th February 2021,
Accepted 5th July 2021

DOI: 10.1039/d1cp00657f

rsc.li/pccp

On the basis of the first-principles evolutionary crystal structure prediction of stable compounds in the Cu–F system, we predict two experimentally unknown stable phases – Cu_2F_5 and CuF_3. Cu_2F_5 comprises two interacting magnetic subsystems with Cu atoms in the oxidation states +2 and +3. CuF_3 contains magnetic Cu^{3+} ions forming a lattice by antiferromagnetic coupling. We showed that some or all of Cu^{3+} ions can be reduced to Cu^{2+} by electron doping, as in the well-known $KCuF_3$. Significant similarities between the electronic structures calculated in the framework of DFT+U suggest that doped CuF_3 and Cu_2F_5 may exhibit high-T_c superconductivity with the same mechanism as in cuprates.

1 Introduction

Transition metal fluorides have been thoroughly studied during the last century.[1,2] Among them, coinage metal fluorides have recently attracted considerable attention: the Cu–F system in the electrochemistry field,[3–6] Ag–F as a potential new route to superconductivity,[7,8] and Au–F due to the unusual oxidation state of gold.[9] Actually, the Cu–F system contains an old puzzle of crystalline copper fluoride existence and synthesis, which produced a never-ending debate and remained unresolved to date. The first report of the synthesis of CuF with a zinc blende structure was published in 1933.[10] It was then argued that the reported CuF is identical to Cu_2O, dismissing the previous experimental results.[11] Recently, no one succeeded in reproducing the synthesis of CuF, and the earliest studies have met strong criticism,[12,13] since it is commonly believed that fluorine, because of its high electronegativity, will always oxidize copper to the oxidation state +2. Even though all attempts to synthesize CuF have been unsuccessful and the very existence of this compound is questionable, studies are ongoing,[14,15] and the complexes of CuF are already well characterized.[16]

The computationally guided studies of new transition metal fluorides, and CuF in particular, also continue. Initially, they mainly compared different structure prototypes to find a hypothetical ground state crystal structure[17,18] or investigated cluster formation.[19] A variety of new structures have been reported using evolutionary crystal structure prediction and assuming CuF stoichiometry.[20] On the basis of all previous studies, eventually, it has been shown that all the predicted structures are metastable.[18,20]

Recently, a computational crystal structure prediction of coinage metal fluorides at different pressures has been done.[9] However, the used method works with a fixed stoichiometry, which limits the prediction of new phases in the whole system. Moreover, redoing the same calculations leads to different structures.[21] Thus, a detailed and reliable analysis of the whole Cu–F system remains to be carried out.

In this work, we present a first-principles variable-composition evolutionary crystal structure prediction study of all phases in the Cu–F system. We recover the experimentally known structure of CuF_2 and report hitherto the unknown stable $C2/m$-Cu_2F_5, $R\bar{3}c$-CuF_3, and $Pnma$-CuF_3 phases. Based on the similarities between the crystal structure of the discovered fluorides and the structure of the parent cuprate high-temperature (high-T_s) superconductor La_2CuO_4, we explored the possibility of high-T_s superconductivity in doped copper fluorides.

2 Computational methods

Here, the stable phases in the Cu–F system were predicted using the first-principles evolutionary algorithm as implemented in the USPEX package.[22,23] The evolutionary search was combined with structure relaxation and energy calculations using density functional theory (DFT) within the Perdew–Burke–Ernzerhof (PBE)[24] exchange–correlation functional and employing the projector augmented plane wave (PAW) method[25] as implemented in

[a] *Skolkovo Institute of Science and Technology, 30 Bolshoy Boulevard, bld. 1, Moscow 121205, Russia. E-mail: Nikita.Rybin@skoltech.ru, D.Novoselov@skoltech.ru, A.Oganov@skoltech.ru*
[b] *M. N. Mikheev Institute of Metal Physics of Ural Branch of Russian Academy of Sciences, 18 S. Kovalevskaya St., Yekaterinburg, 620137, Russia*
[c] *Department of Theoretical Physics and Applied Mathematics, Ural Federal University, 19 Mira St., Yekaterinburg 620002, Russia*

† Electronic supplementary information (ESI) available: Optimized structural parameters, total energies, and phonon dispersion curves of novel structures; DOS for $Pnma$-CuF_3; schematic representation of the crystal structure of $Im\bar{3}m$-$K_{0.75}CuF_3$. See DOI: 10.1039/d1cp00657f

the VASP package.[26] We used a plane-wave energy cutoff of 600 eV and Γ-centered k-meshes with a resolution of $2\pi \times 0.05$ Å^{-1} for Brillouin zone sampling, ensuring the excellent convergence of the quantities of interest. During the variable-composition structure search, the first generation of 160 structures was produced using random symmetric[27] and random topological[28] structure generators, with up to 18 atoms in the primitive cell. 70% of the next generation was obtained by applying variation operators (heredity, soft mutation, lattice mutation) to the 70% of the lowest energy structures of the current generation and the other 30% of the generation was produced randomly.

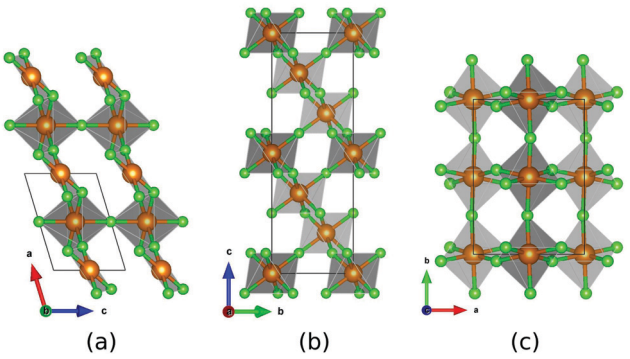

Fig. 2 Schematic representation of the crystal structures: (a) $C2/m$-Cu_2F_5, (b) $R\bar{3}c$-CuF_3, and (c) $Pnma$-CuF_3. Cu and F atoms are shown in brown and green, respectively. Structures were visualized using VESTA.[34]

3 Results and discussion

3.1 Hitherto unknown compounds in the Cu–F system

Phases located on the thermodynamic convex hull are stable with respect to decomposition into elemental Cu and F or other Cu–F compounds. Moreover, all the values of the chemical potentials, delimiting the fields of stability of compounds, are derived directly from the convex hull. The spin-polarized DFT calculations lead to the convex hull diagram of the Cu–F system as presented in Fig. 1. It contains experimentally known $P2_1/c$-CuF_2, hitherto unknown $C2/m$-Cu_2F_5 and $R\bar{3}c$-CuF_3, and slightly metastable $Pnma$-CuF_3, which is just 0.001 eV above the convex hull. The successful prediction of CuF_2, a known compound, and $R\bar{3}c$-CuF_3, predicted in another theoretical study,[9] indicates the robustness of our methodology for crystal structure prediction. All the obtained potentially stable structures became the subject of an additional fixed-composition study taking into account up to four formula units (and up to 18 atoms in the unit cell for CuF). The dynamical stability of all the structures was carefully verified with phonon calculations using the supercell approach and finite isplacement method, as implemented in the Phonopy package.[29] The structural information for the obtained compounds and the phonon dispersion curves are presented in the ESI.†

The most energetically favorable structure of CuF, found in our study, is the low-symmetry $P\bar{1}$-CuF, which is even lower in energy than that in previous reports[20] by ~0.05 meV per atom, but its low symmetry and high energy (~50 meV per atom above the convex hull) indicated its instability and tendency to decompose into Cu + CuF_2. Thus, we conclude that CuF is unlikely to exist at ambient pressure.

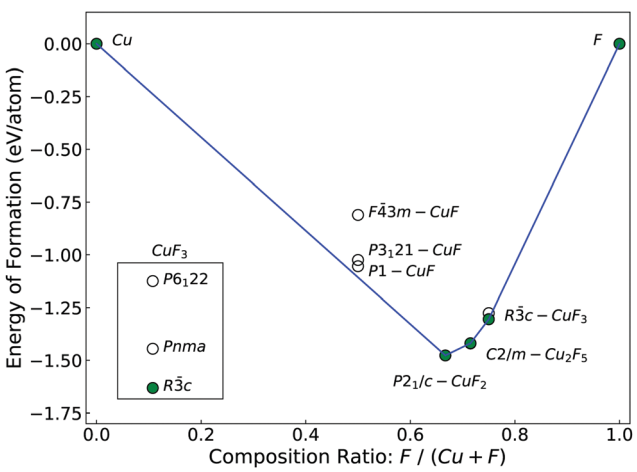

Fig. 1 Convex hull diagram of the Cu–F system. The inset schematically presents the existence of three CuF_3 phases.

Cu_2F_5 crystallizes in the monoclinic space group $C2/m$ with two inequivalent Cu sites, where each Cu atom of the first type is bonded to six pairwise equivalent F atoms forming a CuF_6 octahedron (Fig. 2a), with the corner-sharing octahedral tilt angles of 0°. In the second site, the Cu atom is in a square planar geometry with four pairwise equivalent F atoms. This arrangement could also be described as a distorted octahedron (see the ESI† Fig. S3a). While isostoichiometric $P\bar{1}$-Ag_2F_5 is well-known,[7] hypothetical $P\bar{1}$-Cu_2F_5 has a higher energy than $C2/m$-Cu_2F_5 by ~3 meV per atom in the spin-polarized DFT solution.

Ground state CuF_3 has a trigonal perovskite structure with the space group $R\bar{3}\,c$ (Fig. 2b). This structure was also predicted in ref. 9. The Cu atom is bonded with six equivalent F atoms to form an octahedron with the corner-sharing octahedral tilt angles of 29°. Orthorhombic $Pnma$-CuF_3, metastable at 0 K, also has a perovskite structure ABX_3 with the absence of A cations – ReO_3-type structure (Fig. 2c), with the corner-sharing octahedral tilt angles of 28°. Metal trifluorides such as FeF_3, CoF_3, RuF_3, RhF_3, PdF_3, and IrF_3 also have a perovskite structure with the space group $R\bar{3}c$,[30] whereas AgF_3 and AuF_3 crystallize in a totally different structure with the space group $P6_122$.[31,32] Hypothetical $P6_122$-CuF_3 has a higher energy than the $R\bar{3}c$ phase by ~30 meV per atom in the spin-polarized DFT solution. Notably, perovskite-type structures frequently have octahedral tilt instabilities and exhibit phase transition.[33]

3.2 Analogy with cuprates

Discovered Cu fluorides have significant crystal-chemical similarities with high-T_s cuprates. In both systems, we observe Cu^{2+} (in square planar coordination, as a consequence of Jahn–Teller distortion in all cuprates and Cu_2F_5) and Cu^{3+} (in CuF_3, Cu_2F_5, and doped cuprates). As we discuss below, pure parent compounds CuF_3, Cu_2F_5, and La_2CuO_4 are antiferromagnetic insulators, but doping with electrons or holes makes them metallic and superconducting (for sure La_2CuO_4, and most likely for copper fluorides).

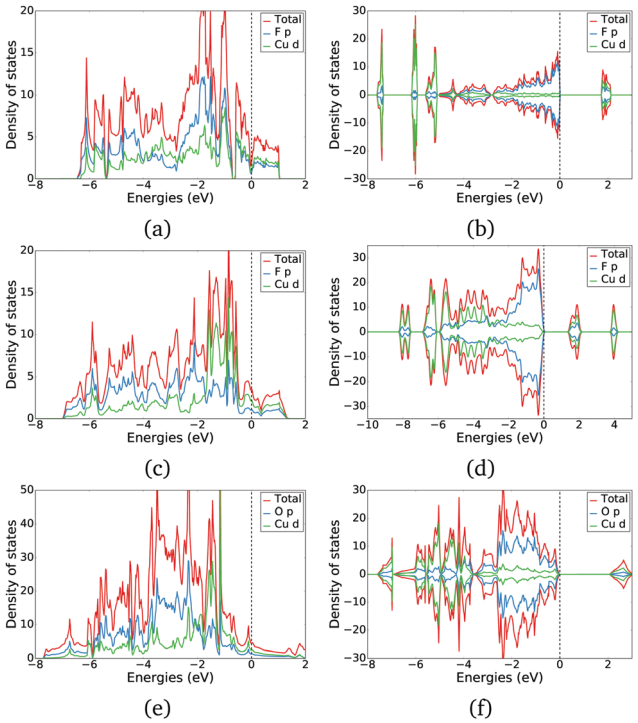

Fig. 3 Total and partial density of states for (a and b) $R\bar{3}c$-CuF_3, (c and d) Cu_2F_5, and (e and f) *Bamb*-La_2CuO_4 obtained using (a, c and e) DFT and (b, d and f) DFT+*U*.

To compare the electronic properties of copper fluorides and cuprates, we first performed the spin-unpolarized DFT calculations using dense Monkhorst–Pack meshes of 8 × 8 × 4 and 12 × 12 × 12 *k*-points for the distorted orthorombic low-temperature *Bamb*-La_2CuO_4 phase and all fluorides, respectively. Structural information and energies for ferromagnetic and antiferromagnetic orders are presented in the ESI† (Tables S1 and S2). The density of states (DOS) for $R\bar{3}c$-CuF_3, Cu_2F_5, and *Bamb*-La_2CuO_4 resolved for the Cu-d and ligand-p states using DFT is shown in Fig. 3(a, c and e). In all the systems, the DFT results show that the Cu-3d energy band is located completely inside the p band of the ligands and strongly hybridizes with it. Therefore, the partially filled electronic states of interest are formed by the *d*- and *p*-symmetry states with approximately equal weights, and the usual ionic picture is not applicable for such a band structure. Notably, the magnetic exchange interaction is proportional to the scale of magnetic fluctuations. For all the considered systems, solutions with antiferromagnetic order are the lowest in energy (ESI† Tables S3 and S4).

Since the energy difference obtained from the spin-unpolarized and spin-polarized DFT calculations is quite small (comparable to the thermal energy at room temperature (~26 meV) and vibrational energy of atoms (the highest optical phonon modes have energies of ~75 meV in Cu_2F_5 and ~65 meV in CuF_3 and less than ~0.05 and ~0.1 eV per Cu atom for Cu_2F_5 and CuF_3, correspondingly, and ~10^{-4} eV per Cu atom for $K_{0.75}CuF_3$)), one can expect strong spin fluctuations in both types of systems – and we recall that the high-T_c superconductivity of cuprates is believed to be mediated by spin fluctuations. Doped Cu fluorides can, or perhaps, be superconducting by the same magnetically mediated mechanism.

3.3 The importance of DFT+*U*

Although DFT sheds light on some premature analogies with cuprates, in principle, this method is pathological since it cannot correctly reproduce the antiferromagnetic insulating state of La_2CuO_4 because it neglects on-site Coulomb correlations,[35] and more robust results are achieved by taking into account the electronic correlations using the DFT+*U* method with the Coulomb interaction parameter U = 8 eV and the exchange interaction parameter J = 0.9 eV.[35,36] Because we deal with copper in the same divalent and trivalent states, and the energy bands in cuprates and copper fluorides studied here have similar widths (Fig. 3a, c, e and Table 1), we chose the same values of U and J for all the calculations taking into account the on-site Coulomb repulsion between the Cu-3d electrons in CuF_3, Cu_2F_5, and *Bamb*-La_2CuO_4. For consistency with DFT calculations, the PBE exchange–correlation functional was also used in DFT+*U*. Structural information obtained after the relaxation with DFT+*U* and the values of total energy for ferromagnetic and antiferromagnetic orders are presented in the ESI† (Tables S1 and S2). We note that the calculations at the DFT-PBE level of theory allow us to compare the formation energy of structures on equal footing during the crystal structure prediction step. The inclusion of correlation effects at this step would require some particular U, which would be suitable for all compounds in the search. In fact, such U does not exist.

We reproduced the insulating antiferromagnetic ground state of *Bamb*-La_2CuO_4 with the DFT+*U* energy gap of about 2 eV and the magnetic moment of the Cu atoms of 0.65 μ_B, which are in close agreement with the experimentally observed values of ~2 eV and 0.68 μ_B, respectively.[37] The DOS for $R\bar{3}c$-CuF_3, Cu_2F_5, and *Bamb*-La_2CuO_4 obtained using DFT+*U* is presented in Fig. 3(b, d and f). The DOS for the *Pnma* phase is presented in Fig. S2a and b in the ESI†. For $R\bar{3}c$-CuF_3 and *Pnma*-CuF_3 in the antiferromagnetic phase, the DFT+*U* calculations show similarities in the key features of the electronic structures of CuF_3 and *Bamb*-La_2CuO_4 – they have well-separated Hubbard bands formed by the Cu-d states, whereas the first ionization states have a *p*-symmetry and are formed by the ligands.

In the CuF_3 structures, copper has an atypical formal oxidation state of +3, which leads to the $3d^8$ electronic configuration, whereas in *Bamb*-La_2CuO_4 there are Cu^{2+} Jahn–Teller active ions. However, some or all of Cu^{3+} ions in CuF_3 can be reduced to Cu^{2+} by electron doping, like in the well-known perovskite-type $KCuF_3$, where all Cu atoms are in the oxidation state +2. CuF_3, in fact, can

Table 1 Bandwidth W and charge transfer gap Δ_{pd} calculated using DFT. Hubbard bands splitting U_{dd}, spin S, and magnetic moment M obtained using the DFT+*U* method. The values in parentheses are related to the second type of Cu atoms in the Cu_2F_5

	W (eV)	Δ_{pd} (eV)	U_{dd} (eV)	S	M (μ_B)
$R\bar{3}c$-CuF_3	8	1.7	9.5	1	1.15
Cu_2F_5	8	1.42	9.5	1 (1/2)	1.17 (0.79)
La_2CuO_4	9	2	10.5	1/2	0.65

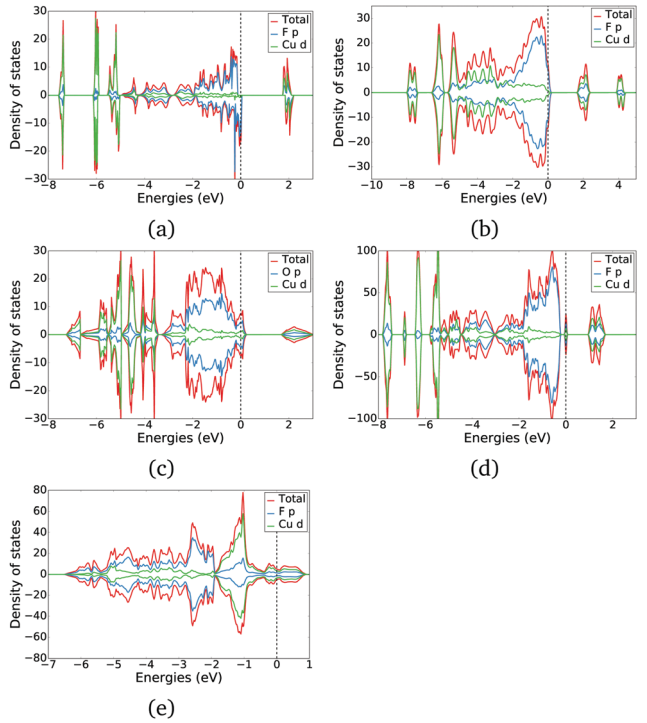

Fig. 4 Total and partial density of states for p-doped (a) $R\bar{3}c$-CuF_3, (b) Cu_2F_5, and (c) La_2CuO_4. (d) $R\bar{3}c$-CuF_3 with one *F* vacancy per 2 × 2 × 2 supercell, (e) and perovskite-type $Im\bar{3}m$-$K_3(CuF_3)_4$.

be described as the structure of $KCuF_3$ with all K atoms removed. Thus, one way to make a superconducting Cu fluoride is to remove the part of K atoms from $KCuF_3$ (in a vacuum tube) – the result should be a metallic perovskite-type compound with mixed Cu^{2+} and Cu^{3+} states. To clearly show this, we performed a fixed-composition structure search of $K_3(CuF_3)_4$, which determined that the most stable phase has a perovskite-type structure with the space group $Im\bar{3}m$ (ESI,† Fig. S3c). This structure is stable with respect to the decomposition into $R\bar{3}c$-CuF_3 and $KCuF_3$ (~0.05 eV per atom below the decomposition line), which means that potassium ions can be easily extracted from the $KCuF_3$, forming a mixed-valence compound.

According to the DFT+*U* solution: each Cu site in the CuF_3 has spin 1; Cu_2F_5 is determined as a compound with the mixed-valence Cu^{2+}/Cu^{3+} state and Cu ions with spin 1 and 1/2; Cu ions in the cuprate have spin 1/2. The magnetic moments per Cu atom obtained from the DFT+*U* calculations for $R\bar{3}c$-CuF_3 are 1.15 μ_B (1.14 μ_B in the *Pnma* phase). These magnetic moment values are smaller by a factor of 0.58 than the formal ionic value of 2 μ_B for a Cu^{3+} ion compared to the reduction factor of 0.65 for the formal atomic value of 1 μ_B for a Cu^{2+} ion in the La_2CuO_4.[37] For Cu_2F_5, we found that two types of Cu atoms have different formal electronic configurations of d^8 and d^9, and different magnetic moments of 1.17 μ_B and 0.79 μ_B. All the predicted copper fluoride structures and *Bamb*-La_2CuO_4 are charge-transfer insulators with respect to the classification of Zaanen *et al.*[38] The first energy excitation occurs between the p band of the ligands and the d band of the metal ion. CuF_3 has a small charge transfer gap (an important characteristic of cuprates) Δ_{pd} = 1.7 eV, and Cu_2F_5 also has a small charge transfer gap Δ_{pd} = 1.42 eV, comparable with 2 eV of La_2CuO_4. Though the energy gap depends on the choice of the Hubbard *U* parameter, the charge-transfer nature of the gap remains the same for a wide range of *U* values in fluorides. The splitting between the Hubbard bands for CuF_3 and La_2CuO_4 is similar and equal to ~9.5 eV and 10.5 eV, respectively (Fig. 3b and d).

3.4 Influence of doping on the electronic structure

Cu_2F_5, CuF_3, and La_2CuO_4 are insulators and can exhibit superconductivity only when properly doped. Consequently, we performed DFT+*U* calculations of the considered systems doped with holes using the rigid-band shift approximation, with doping amounted to 0.25 holes for each copper atom in the unit cell (Fig. 4a–c). CuF_3 and Cu_2F_5, like La_2CuO_4, undergo a transition from the insulating to the conducting state upon the hole doping, which once again highlights the similarity of their electronic properties. We have also examined a 2 × 2 × 2 $R\bar{3}c$-CuF_3 supercell (64 atoms) with a vacancy on one of the F atoms. This ferrimagnetic structure lies on the thermodynamic convex hull (Fig. 1). This indicates that the formation of non-stoichiometric CuF_{3-x} is favorable. The DFT+*U* solution determines the formation of a peak at the Fermi level for this structure (Fig. 4d). The perovskite-type $Im\bar{3}m$-$K_3(CuF_3)_4$ also has a metallic solution from the DFT+*U* study (Fig. 4e).

4 Conclusions

In summary, the results of the systematic crystal structure search in the Cu–F system support that CuF is unlikely to exist and have revealed hitherto unknown $C2/m$-Cu_2F_5 and $R\bar{3}c$-CuF_3, and slightly metastable *Pnma*-CuF_3. Cu_2F_5 contains Cu ions with oxidation states +2 and +3, which leads to the presence of two magnetic subsystems. In CuF_3, Cu ions have an unusual oxidation state +3, which can be reduced to +2 by appropriate doping. We showed that potassium can be extracted from $KCuF_3$ forming a metallic state. We showed using DFT+*U* that all the discovered copper fluorides are strongly correlated compounds and charge-transfer insulators. Since the comparison of CuF_3 and Cu_2F_5 with the classical cuprate La_2CuO_4 shows many similarities, the discovered structures could possibly be a new class of high-T_c superconductors.

Conflicts of interest

There are no conflicts to declare.

Acknowledgements

This work was supported by the Russian Science Foundation (Project 19-72-30043). Calculations were performed on Arkuda cluster of Skoltech and Uran cluster of IMM UB RAS. DYN, DMK and VIA thank the Ministry of Science and Higher Education of the Russian Federation (No. AAAA-A18-118020190098-5, topic "Electron").

References

1 J. M. Winfield, *J. Fluorine Chem.*, 1986, **33**, 159–178.
2 J. S. Thrasher and S. H. Strauss, *Inorganic Fluorine Chemistry*, 1994, ch. 1, pp. 1–23.
3 F. Wang, R. Robert, N. A. Chernova, N. Pereira, F. Omenya, F. Badway, X. Hua, M. Ruotolo, R. Zhang, L. Wu, V. Volkov, D. Su, B. Key, M. Stanley Whittingham, C. P. Grey, G. G. Amatucci, Y. Zhu and J. Graetz, *J. Am. Chem. Soc.*, 2011, **133**, 18828–18836.
4 F. Wang, H. C. Yu, M. H. Chen, L. Wu, N. Pereira, K. Thornton, A. Van Der Ven, Y. Zhu, G. G. Amatucci and J. Graetz, *Nat. Commun.*, 2012, **3**, 1–8.
5 X. Hua, R. Robert, L.-S. Du, K. M. Wiaderek, M. Leskes, K. W. Chapman, P. J. Chupas and C. P. Grey, *J. Phys. Chem. C*, 2014, **118**, 15169–15184.
6 F. Omenya, N. J. Zagarella, J. Rana, H. Zhang, C. Siu, H. Zhou, B. Wen, N. A. Chernova, L. F. J. Piper, G. Zhou and M. S. Whittingham, *ACS Appl. Energy Mater.*, 2019, **2**, 5243–5253.
7 W. Grochala and R. Hoffmann, *Angew. Chem., Int. Ed.*, 2001, **40**, 2742–2781.
8 J. Gawraczynski, D. Kurzydłowski, R. A. Ewings, S. Bandaru, W. Gadomski, Z. Mazej, G. Ruani, I. Bergenti, T. Jaron, A. Ozarowski, S. Hill, P. J. Leszczynski, K. Tokár, M. Derzsi, P. Barone, K. Wohlfeld, J. Lorenzana and W. Grochala, *Proc. Natl. Acad. Sci. U. S. A.*, 2019, **116**, 1495–1500.
9 J. Lin, S. Zhang, W. Guan, G. Yang and Y. Ma, *J. Am. Chem. Soc.*, 2018, **140**, 9545–9550.
10 F. Ebert and H. Woitinek, *Z. Anorg. Allg. Chem.*, 1933, **210**, 269–272.
11 H. M. Haendler, L. H. Towle, E. F. Bennett and W. L. Patterson, *J. Am. Chem. Soc.*, 1954, **76**, 2178–2179.
12 C. Housecroft and A. Sharpe, *Inorganic Chemistry*, Pearson Prentice Hall, 2005.
13 N. N. Greenwood and A. Earnshaw, *Chemistry of the Elements*, Elsevier Science, 2012.
14 X. Wang, L. Andrews, F. Brosi and S. Riedel, *Chem. – Eur. J.*, 2013, **19**, 1397–1409.
15 P. Woidy, A. J. Karttunen, M. Widenmeyer, R. Niewa and F. Kraus, *Chem. – Eur. J.*, 2015, **21**, 3290–3303.
16 D. J. Gulliver, W. Levason and M. Webster, *Inorg. Chim. Acta*, 1981, **52**, 153–159.
17 T. Söhnel, H. Hermann and P. Schwerdtfeger, *J. Phys. Chem. B*, 2005, **109**, 526–531.
18 A. Walsh, C. R. A. Catlow, R. Galvelis, D. O. Scanlon, F. Schiffmann, A. A. Sokol and S. M. Woodley, *Chem. Sci.*, 2012, **3**, 2565–2569.
19 R. P. Krawczyk, A. Hammerl and P. Schwerdtfeger, *ChemPhysChem*, 2006, **7**, 2286–2289.
20 M. S. Kuklin, L. Maschio, D. Usvyat, F. Kraus and A. J. Karttunen, *Chem. – Eur. J.*, 2019, **25**, 11528–11537.
21 G. Liu, X. Feng, L. Wang, S. A. Redfern, X. Yong, G. Gao and H. Liu, *Phys. Chem. Chem. Phys.*, 2019, **21**, 17621–17627.
22 A. R. Oganov and C. W. Glass, *J. Chem. Phys.*, 2006, **124**, 244704.
23 A. R. Oganov, A. O. Lyakhov and M. Valle, *Acc. Chem. Res.*, 2011, **44**, 227–237.
24 J. P. Perdew, K. Burke and M. Ernzerhof, *Phys. Rev. Lett.*, 1996, **77**, 3865–3868.
25 P. E. Blöchl, *Phys. Rev. B: Condens. Matter Mater. Phys.*, 1994, **50**, 17953–17979.
26 G. Kresse and J. Furthmüller, *Phys. Rev. B: Condens. Matter Mater. Phys.*, 1996, **54**, 11169–11186.
27 A. O. Lyakhov, A. R. Oganov, H. T. Stokes and Q. Zhu, *Comput. Phys. Commun.*, 2013, **184**, 1172–1182.
28 P. V. Bushlanov, V. A. Blatov and A. R. Oganov, *Comput. Phys. Commun.*, 2019, **236**, 1–7.
29 A. Togo and I. Tanaka, *Scr. Mater.*, 2015, **108**, 1–5.
30 M. A. Hepworth, K. H. Jack, R. D. Peacock and G. J. Westland, *Acta Crystallogr.*, 1957, **10**, 63–69.
31 B. Žemva, K. Lutar, A. Jesih, W. J. Casteel, A. P. Wilkinson, D. E. Cox, B. Robert von Dreele, H. Borrmann and N. Bartlett, *J. Am. Chem. Soc.*, 1991, **113**, 4192–4198.
32 F. W. Einstein, P. R. Rao, J. Trotter and N. Bartlett, *J. Chem. Soc. A*, 1967, 478–482.
33 P. M. Woodward, *Acta Crystallogr., Sect. B: Struct. Sci., Cryst. Eng. Mater.*, 1997, **53**, 32–43.
34 K. Momma and F. Izumi, *J. Appl. Crystallogr.*, 2008, **41**, 653–658.
35 M. T. Czyyk and G. A. Sawatzky, *Phys. Rev. B: Condens. Matter Mater. Phys.*, 1994, **49**, 14211–14228.
36 V. I. Anisimov, F. Aryasetiawan and A. I. Lichtenstein, *J. Phys.: Condens. Matter*, 1997, **9**, 767–808.
37 W. E. Pickett, *Rev. Mod. Phys.*, 1989, **61**, 433–512.
38 J. Zaanen, G. A. Sawatzky and J. W. Allen, *Phys. Rev. Lett.*, 1985, **55**, 418–421.